Controlled-Source Electromagnetic Survey at New Hyde Park, New York

Carlyle Miller,[1] Warren Barrash,[2] William Clement,[3] and
Partha Routh[4]

Technical Report for
U.S. Environmental Protection Agency Grant X-96004601-0

Center for Geophysical Investigation of
the Shallow Subsurface (CGISS)
Department of Geosciences
Boise State University, Boise, Idaho 83725

March 4, 2008

[1]Formerly with CGISS/Department of Geosciences, Boise State University; Currently with MSE Technology Applications, Butte, Montana

[2]CGISS/Department of Geosciences, Boise State University

[3]CGISS/Department of Geosciences, Boise State University

[4]Formerly with CGISS/Department of Geosciences, Boise State University; Currently with Subsurface Technology, Cononco Phillips, Houston, Texas

1 Introduction

Controlled-source electromagnetic (CSEM) data were acquired in order to characterize subsurface geologic variation at a contaminated groundwater site in New Hyde Park, near the Queens-Nassau County boundary on Long Island, New York. The aquifer of interest is composed of glacially derived sands and gravels and thin, discontinuous clay layers. The clay layers play an important role in determining the fate and transport of the contaminated groundwater and thus were the target for this electromagnetic survey. Further details of the CSEM method are provided in Appendix A. In addition to the CSEM survey, natural gamma logging was completed for 10 monitoring wells at the New Hyde Park Site.

Land use at the New Hyde Park site is split between residential and commercial use. The site can be generally described as being heavily urbanized, with limited space for data acquisition. The site presents a challenging environment due to numerous sources of cultural noise including overhead powerlines, buried utilities, and abundant pedestrian and vehicular traffic.

1.1 Previous Work

Several geophysical surveys have been performed in this area including electrical resistance tomography (ERT), electromagnetic induction, and borehole logging using a natural gamma tool. Of these previous surveys, only the natural gamma logging provided consistently useful results. A 2D ERT profile was acquired on a baseball field near the area of interest, and the resulting images from this profile were promising, but when similar profiles were acquired along the more heavily urbanized streets in the area, data quality and repeatability suffered dramatically. The natural gamma logs are useful for determining the depth and thickness of clay layers in the vicinity of the existing boreholes. Where available, the natural gamma logging results will be compared with the results of this CSEM survey, and we note that these data were also used in an attempt to constrain the inversion of the CSEM data. These comparisons and constraints will be discussed in further detail in subsequent sections of this report. Additional details regarding the natural gamma logging are provided in Appendix C.

2 Data Acquisition

This CSEM survey consisted of injecting alternating electrical current at frequencies between 1Hz and 8192Hz via a grounded electric dipole, then measuring the resulting electric field at a number of locations along two receiver profiles. Figure 1 shows the geometry and location of the source and receiver lines. Receiver stations are located approximately 20 meters apart along 2 profile lines. The raw data consist of amplitude and phase of the electric field for each frequency at each station.

Source current transmission was accomplished using a Zonge GGT-25 Transmitter, controlled by a Zonge XMT-16 Transmitter controller, and powered by a Geotronics 4KW generator. This equipment was used to transmit current into an approximately 1100 meter-long surface-laid wire. The transmitter electrodes were constructed at each end of the dipole by lining approximately 0.5-meter deep soil pits with aluminum foil, then refilling the pit and saturating the surrounding soil with salt water. The wire was then attached directly to the aluminum foil. In order to achieve a stronger transmitted signal, these electrodes were later augmented by wiring several grounded rebar and copper stakes in parallel, then attaching these to the transmitter wire as well. Using this configuration, the source current was transmitted at 1.4-3.8 Amperes at the following frequencies: 1, 2, 4, 8, 16, 32, 64, 128, 256, 512, 1024, 2048, 4096, and 8192 Hz.

We used a Zonge GDP-16 receiver with 5 data acquisition channels for data stacking and recording. Receiver electrodes were copper-copper sulfate ceramic porous pot electrodes emplaced on bare dirt. Receiver line 1 was acquired on 25 July 2007 along North 3rd Street, beginning near Hillside Avenue then going south. Receiver line 2 was acquired on 26 July 2007 along Willis Avenue, starting near Hillside Avenue then proceeding south. Each receiver line consisted of 30 stations; station spacing and receiver dipole length were approximately 20 meters.

Included with this report is a CD containing archival copies of the raw CSEM data acquired for this project. Additional contents of this CD include the following:

- PDF copy of this report

- PDF copies of report figures

- Processed CSEM data (readable by spreadsheet software)

Figure 1: Arial photo/street map of the New Hyde Park site showing the location of the transmitter and the receiver lines, the line on the far left is Line 2, the middle line is Line 1, and the red line on the right is the transmitter. The region that is outlined with the dashed yellow box is shown in greater detail in Figure 2. This image is from Google Earth (earth.google.com).

- Station spreadsheet with receiver and transmitter coordinates

- Raw gamma logging data

- Processed gamma logging data (readable by spreadsheet software)

- Miscellaneous photographs of data acquisition

3 Inverse Modeling

The inverse modeling consists of solving an optimization problem in order to find an electrical conductivity model that reproduces the electric field data to an acceptable level (i.e. the model ideally will not reproduce the noise in the
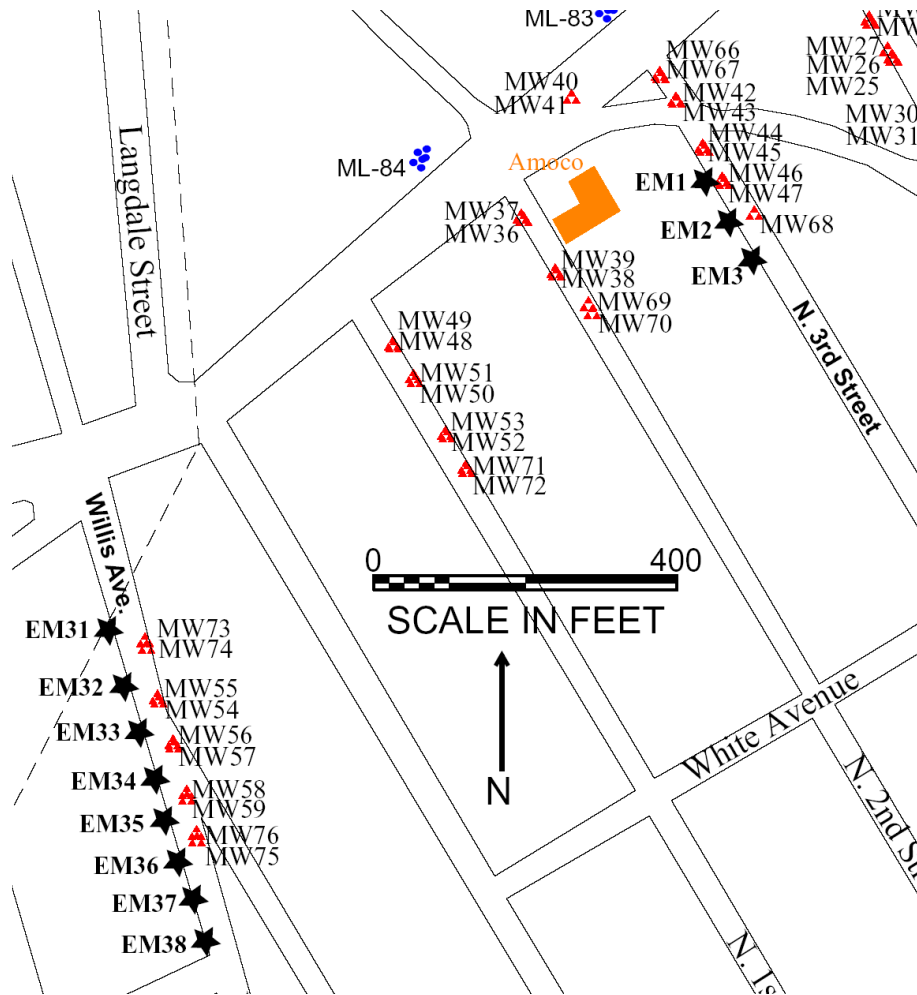
Figure 2: Locations of monitoring wells and selected CSEM stations in the New Hyde Park area. For this study, the monitoring wells of interest are MW-67 and MW-68 located along North 3rd Street, and MW-74 and MW-76 located along Willis Avenue. Only those CSEM stations that were located near monitoring wells are indicated on the map. The dashed line running generally North-South is the Queens-Nassau County Boundary. Map courtesy of Environmental Assessment & Remediations Inc.

data). All modeling has been done in 1D, thus the data from each station are inverted separately. Additional details regarding 1D CSEM inversion are provided in Appendix B. Here is a description of some of the parameter adjustments and inversion strategies that have been applied to the analysis and modeling of these data.

3.1   Layer Parameterization

There are two common techniques for parameterizing the subsurface into layers.

1. Using a set number of layers (80 - 100) with thickness increasing with depth. This is a default setting that is often very effective.

2. Defining a layer parameterization manually, for example 1 meter layers for the first 100 meters, then increasing in thickness from there. This approach was used to "poll" the data for thin clay layers at various depths.

3.2   Band Limited Inversion

This approach inverts a narrower band of frequencies, rather than all 14 frequencies.

1. Inverting lower frequency bands provides information about gross overall structure, and structure at depth.

2. Inverting higher frequency bands provides higher resolution of structure but is insensitive to deep structure.

3. This approach provides a means to determine which data likely are more noise contaminated.

3.3   Cascaded Inversion

This method is similar to band limited inversion, but incorporates information from all frequencies into the final model.

1. Starting with lowest frequency band, invert for a model, then use this model as starting/reference model for inversion of next higher frequency band.

2. Conceptually, structure is built up from a gross scale to a fine scale, and from deep to shallow subsurface positions.

3.4   Starting/Reference Model

1. Half-space reference model makes almost no assumption about structure.

2. More complicated starting/reference model makes some assumption about structure/contrast in conductivity at a specific depth range.

3.5   Model Conditioning

1. Using gamma logs from wells, build a starting/reference model based on peaks in gamma logs that correspond to clay layers. This approach is most useful for stations in close proximity to the well that the log came from.

2. More generally, build starting/reference model with clay layers at various depths, and if the data support the existence of these layers, they should be retained in the final model.

3.6   Smoothness, Flatness of Model

1. Smoothness parameter is used to penalize sharp jumps in the model.

2. Flatness parameter is used to penalize variations from starting/reference model.

3.7   Noise Assumptions

1. We can assign high uncertainty to data that are determined to be noisy, then misfits of these data are penalized less by the inversion.

2. An important caveat is that if noise levels are assumed to be too high, there will be a lack of structure in the final model.

4   Results

The data acquired at New Hyde Park are generally noisy and thus difficult to model. We achieved the best results using a cascaded inversion approach. We first inverted the 5 lowest frequencies (1, 2, 4, 8, 16 Hz). These data are sensitive to the deepest structure. We used the model from this inversion as the starting/reference model for the next five frequencies, with an overlap of one frequency (16, 32, 64, 128, 256 Hz). Finally, we took the model from this inversion as the starting/reference model for the 6 highest frequencies, again with an overlap of one frequency (256, 512, 1024, 2048, 4096, 8192 Hz). The final models from this cascaded approach are presented here. Note that resolution decreases with depth, this is common to almost any electrical method. Also note that resolution is limited by the noise in the data, i.e. if the model contains too much structure, we are possibly fitting noise rather than data. For this reason, the models presented here are all relatively smooth.

We looked at three main criteria to choose which models to include here (Figure 3). First we looked at the models to see if they were geologically reasonable. Several models were discarded based on this criterion either because they were too smooth, i.e. there was no real discernable structure in the model, or because they were too rough, i.e. unrealistic discontinuities in resisitivity between adjacent layers. Next, we looked at the resolution operator to determine whether the region of interest (in this case, the region from the surface to approximately 150 meters depth) was sufficiently resolved by the available data. Most models satisfied this criterion because we had a sufficient frequency range in our data. Lastly, we looked at the fit to the data. We especially focused on the data fit for the higher frequencies, which contain more information about the upper 150 meters of the subsurface. We have divided the results into three subgroups, based on how well these higher frequencies in the data were fit.

4.1   Very Good Data Fit

Stations 13 (Figure 4), 16 (Figure 5), and 37 (Figure 6) had a very good fit to the higher frequency data.
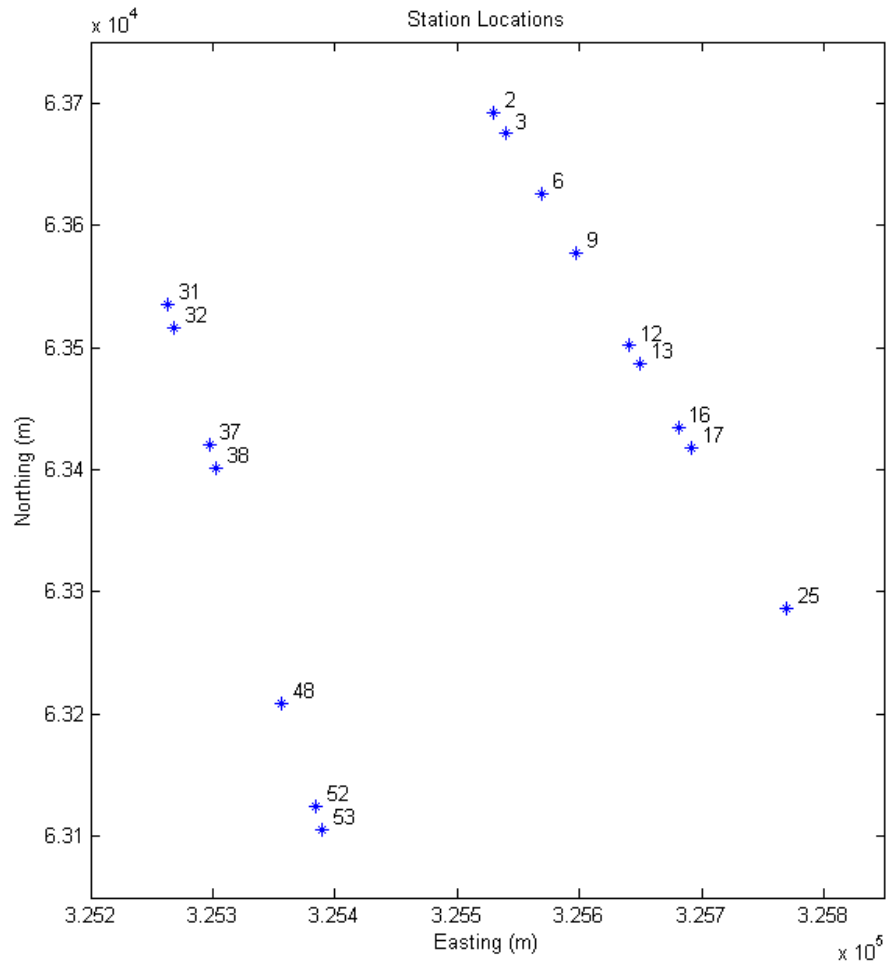
Figure 3: Map showing the locations of stations for which models are presented.
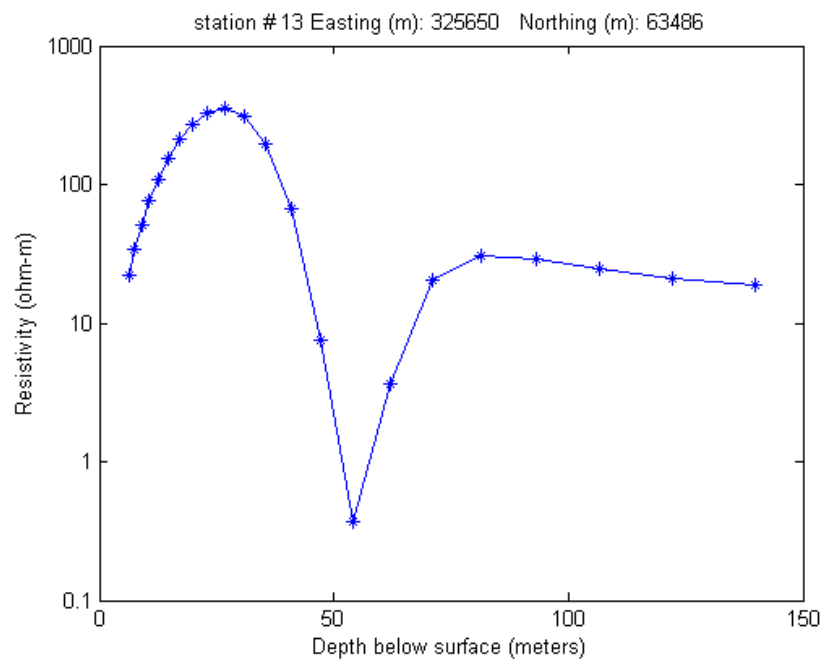
Figure 4: Electrical resistivity model for station 13, note the indication of a possible clay layer at 55 meters depth.

station # 16 Easting (m): 325681   Northing (m): 63435
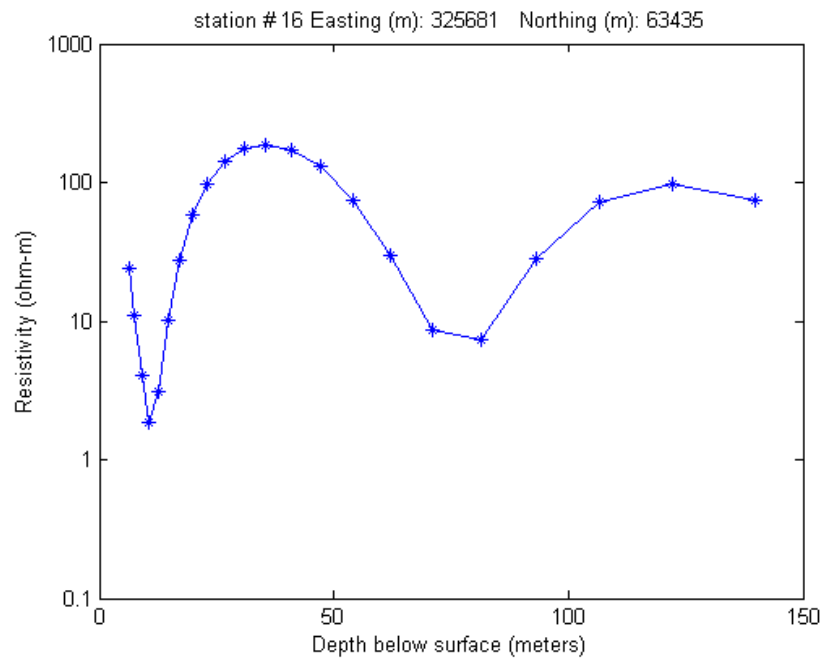
Figure 5: Electrical resistivity model for station 16, note the indication of a possible clay layer at 70-80 meters depth. Additionally, there is a decrease in resistivity at approximately 15 meters, likely associated with the water table.
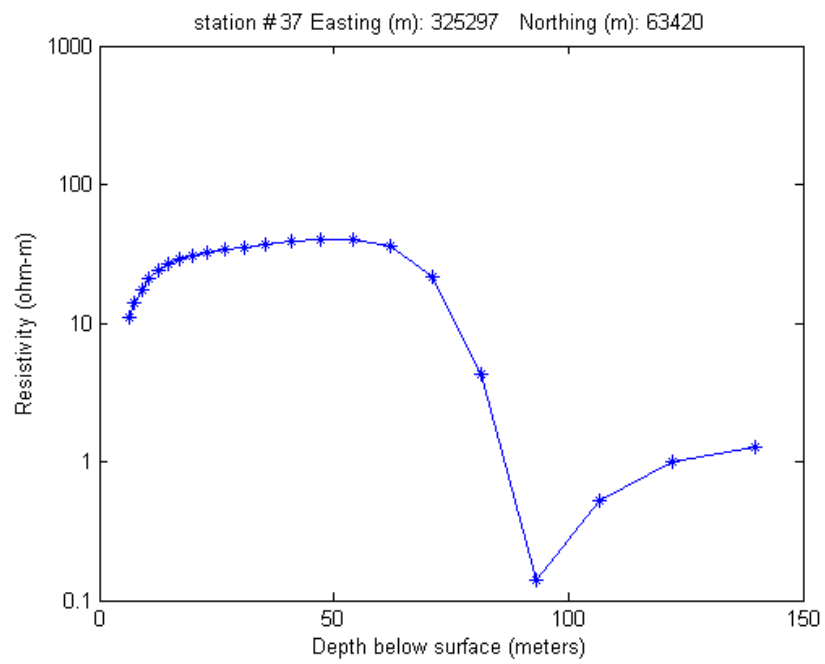
Figure 6: Electrical resistivity model for station 37, note the indication of a possible clay layer at 95 meters depth.
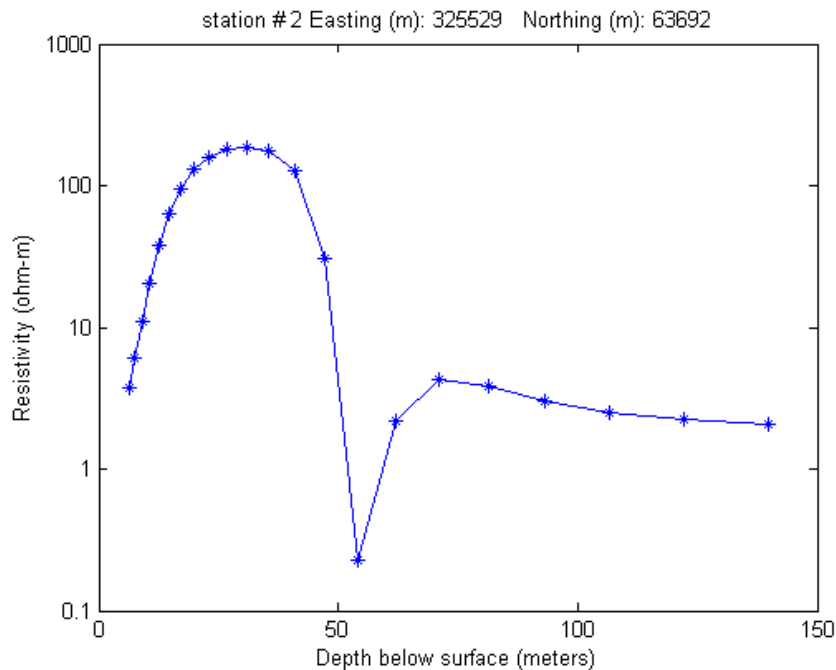
Figure 7: Electrical resistivity model for station 2, note the indication of a possible clay layer at 52 meters depth.

4.2 Reasonably Good Data Fit

Stations 2 (Figure 7), 3 (Figure 8), 31 (Figure 9), and 52 (Figure 10) had a reasonably good fit to the higher frequency data.

4.3 Partially Good Data Fit

Stations 6 (Figure 11), 9 (Figure 12), 12 (Figure 13), 17 (Figure 14), 25 (Figure 15), 32 (Figure 16), 38 (Figure 17), 48 (Figure 18), and 53 (Figure 19) had an overall inadequate fit to the higher frequency data, although some individual frequencies were fit well.
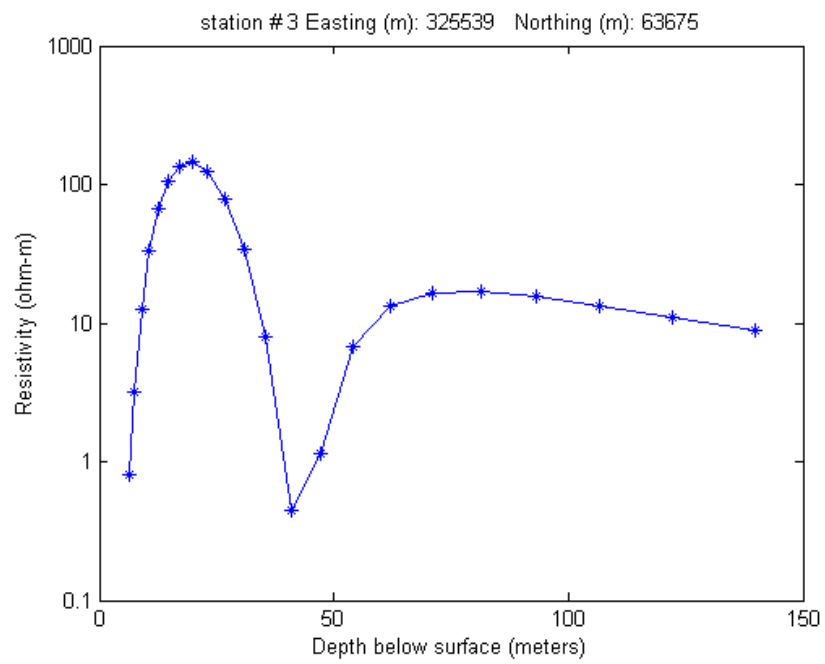
Figure 8: Electrical resistivity model for station 3, note the indication of a possible clay layer at 45 meters depth.
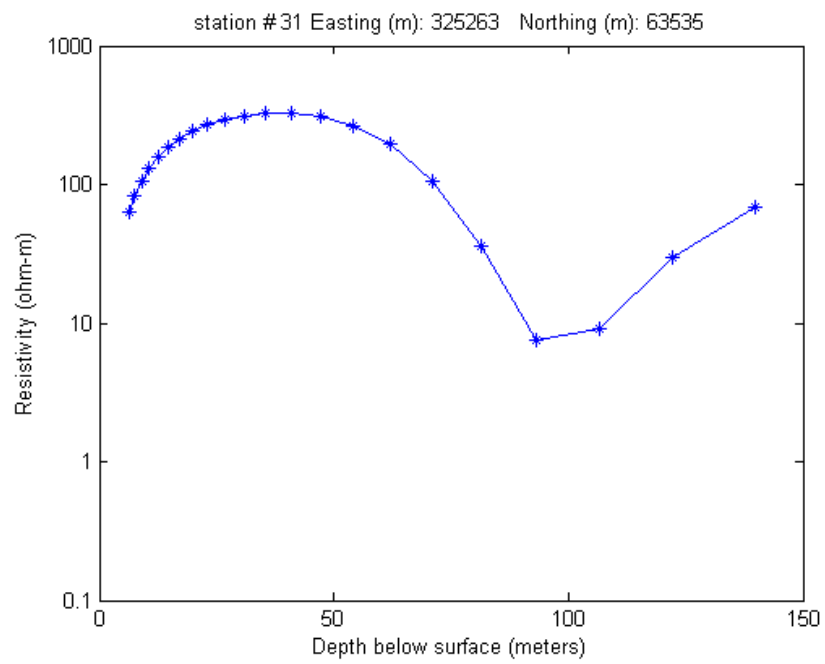
Figure 9: Electrical resistivity model for station 31, note the indication of a possible clay layer at 95-105 meters depth.
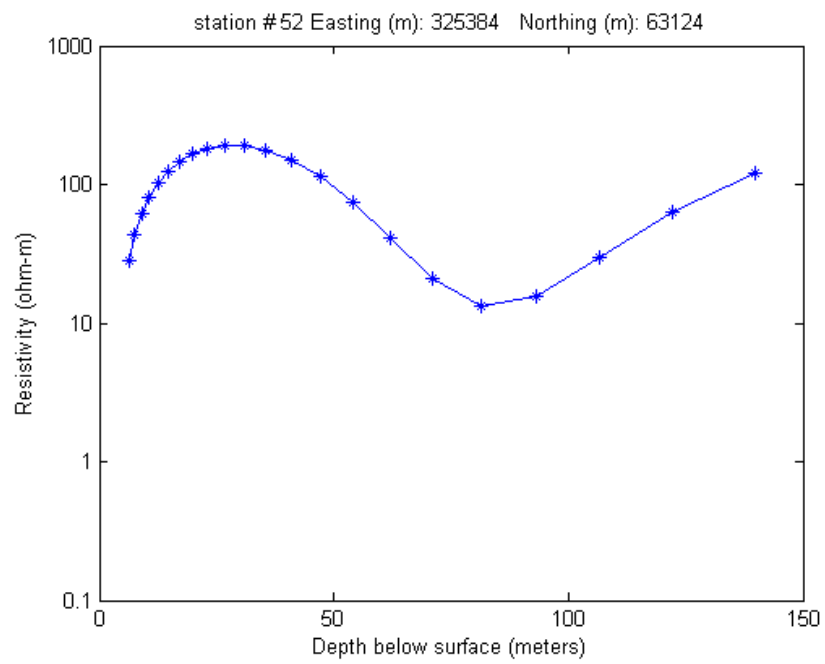
Figure 10: Electrical resistivity model for station 52, note the indication of a possible clay layer at 80 meters depth.

station #6 Easting (m): 325569   Northing (m): 63626
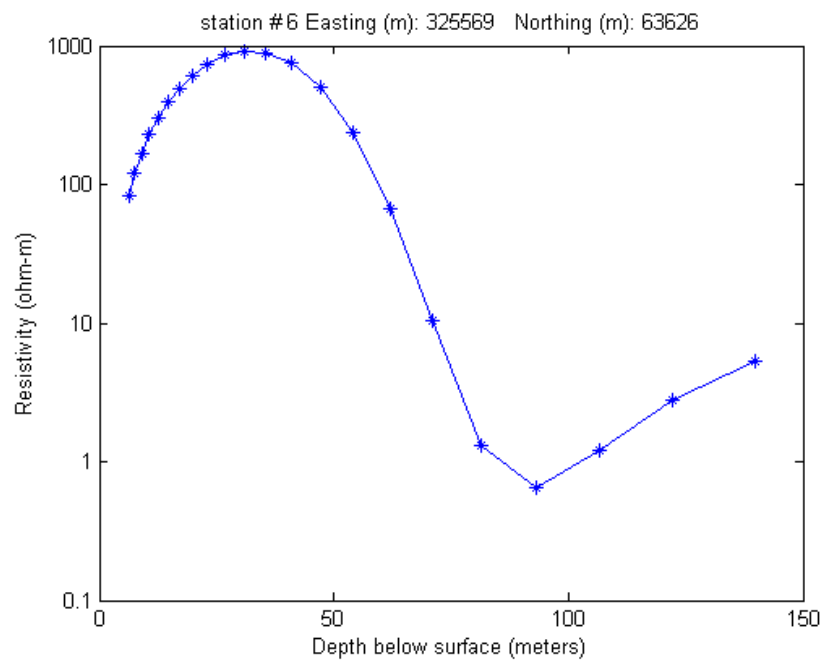
Figure 11: Electrical resistivity model for station 6, note the indication of a possible clay layer at 95 meters depth.
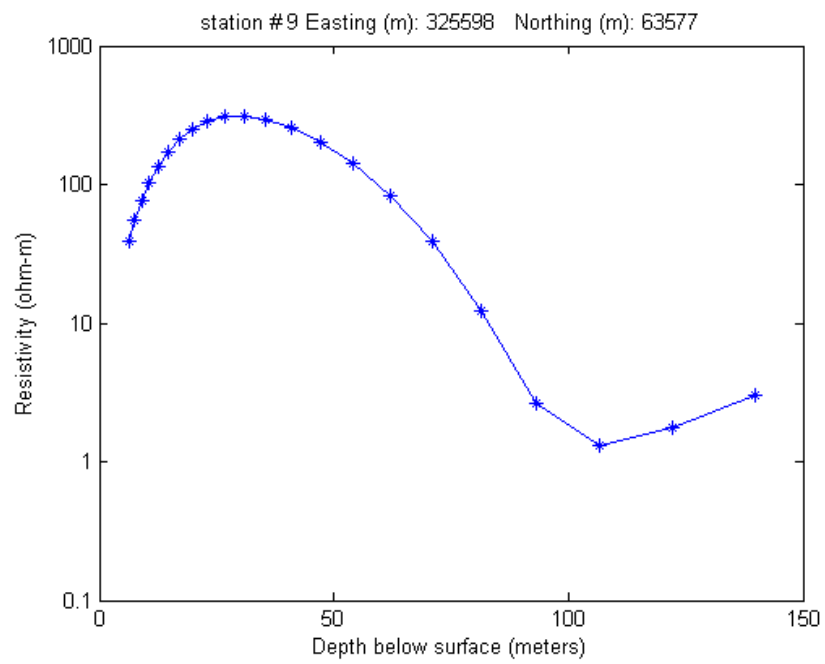
Figure 12: Electrical resistivity model for station 9, note the indication of a possible clay layer at 105 meters depth.
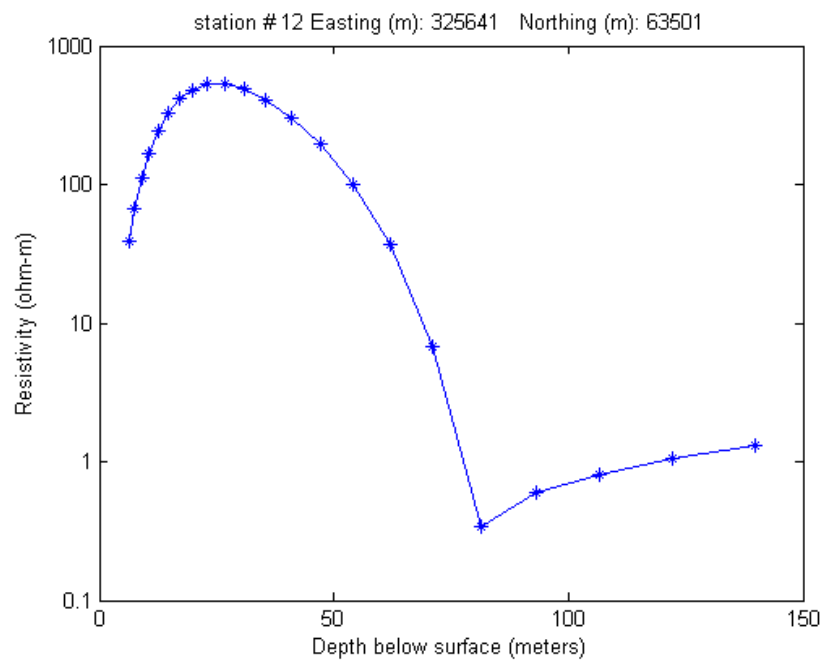
Figure 13: Electrical resistivity model for station 12, note the indication of a possible clay layer at 80 meters depth.
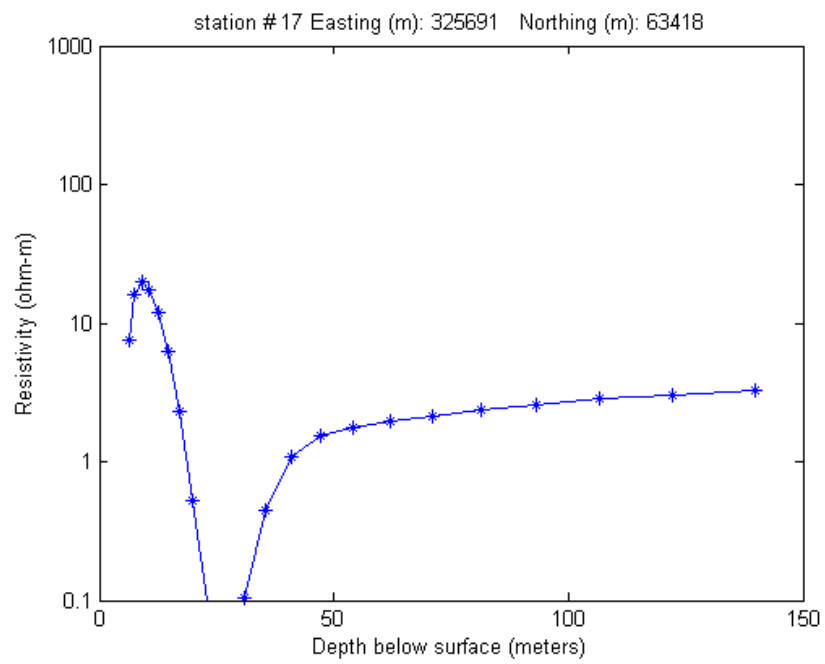
Figure 14: Electrical resistivity model for station 17, note the indication of a possible clay layer at 25 meters depth.
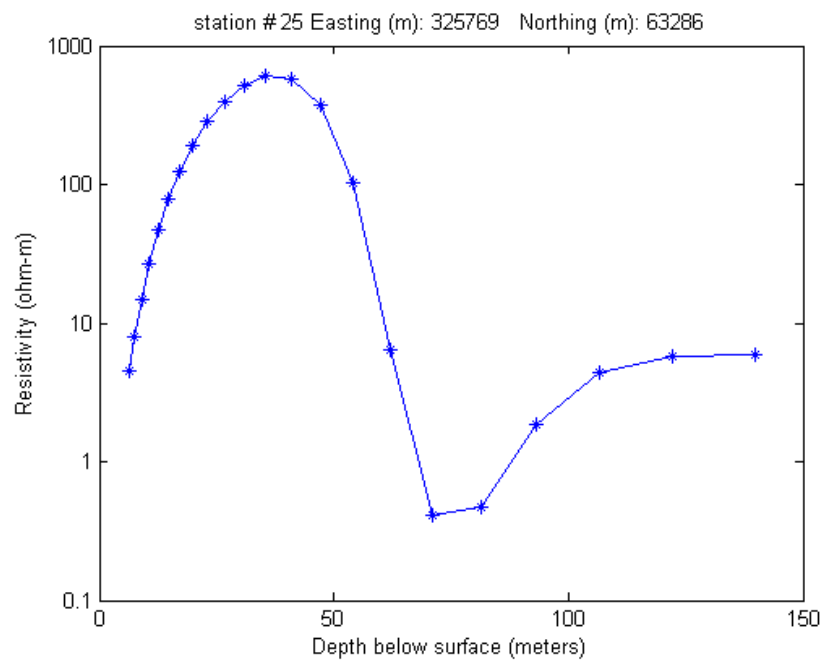
Figure 15: Electrical resistivity model for station 25, note the indication of a possible clay layer at 70-80 meters depth.
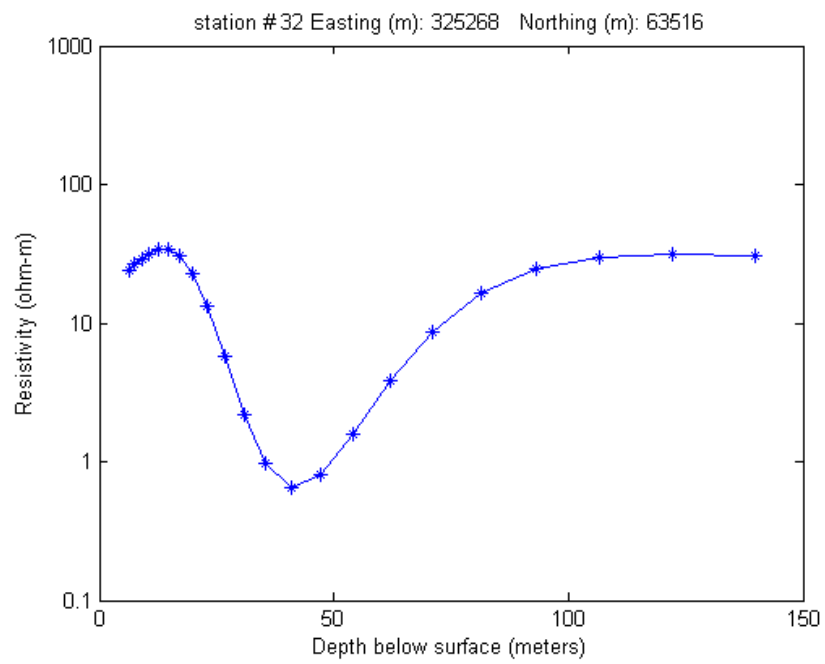
Figure 16: Electrical resistivity model for station 32, note the indication of a possible clay layer at 45 meters depth.
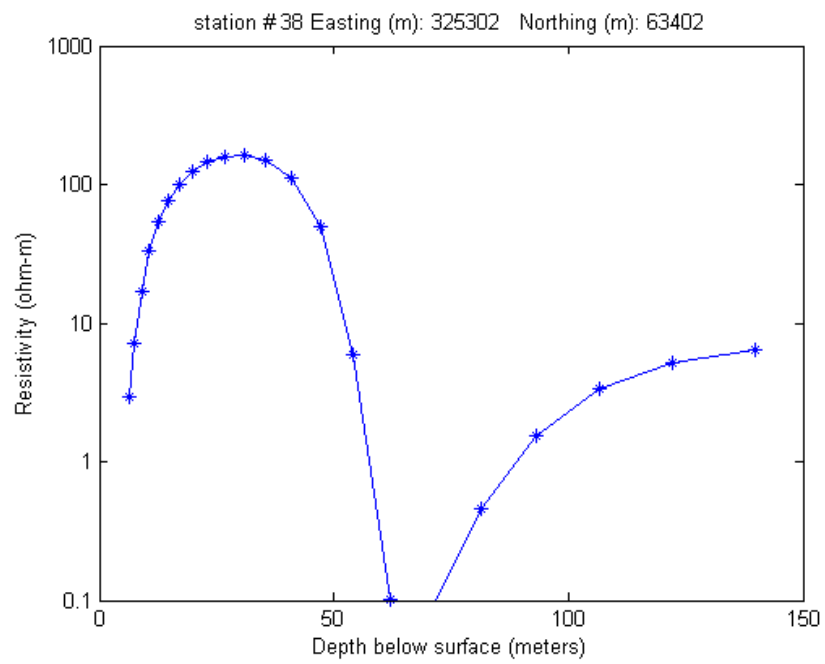
Figure 17: Electrical resistivity model for station 38, note the indication of a possible clay layer at 65 meters depth.

station # 48 Easting (m): 325356   Northing (m): 63209
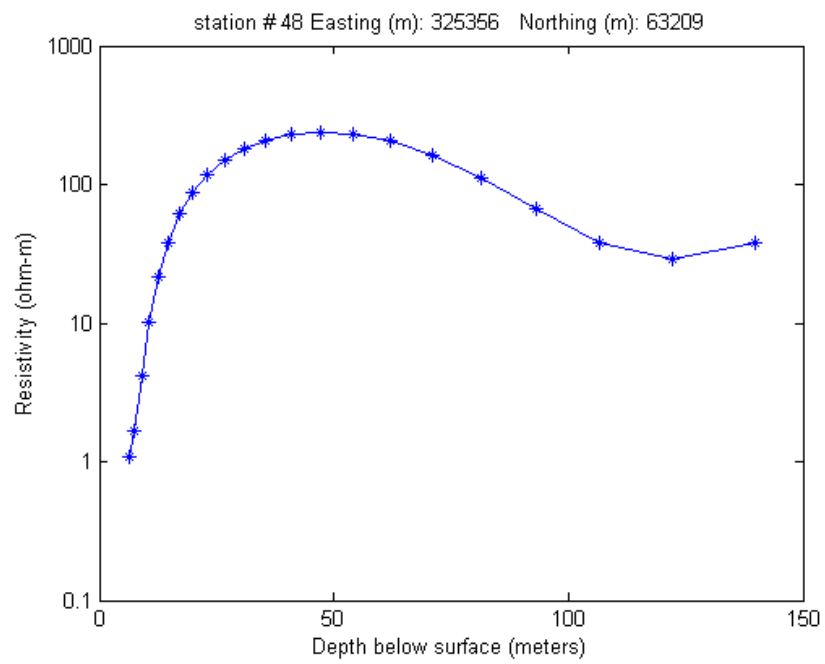
Figure 18: Electrical resistivity model for station 48, note the indication of a possible clay layer at 125 meters depth.

24
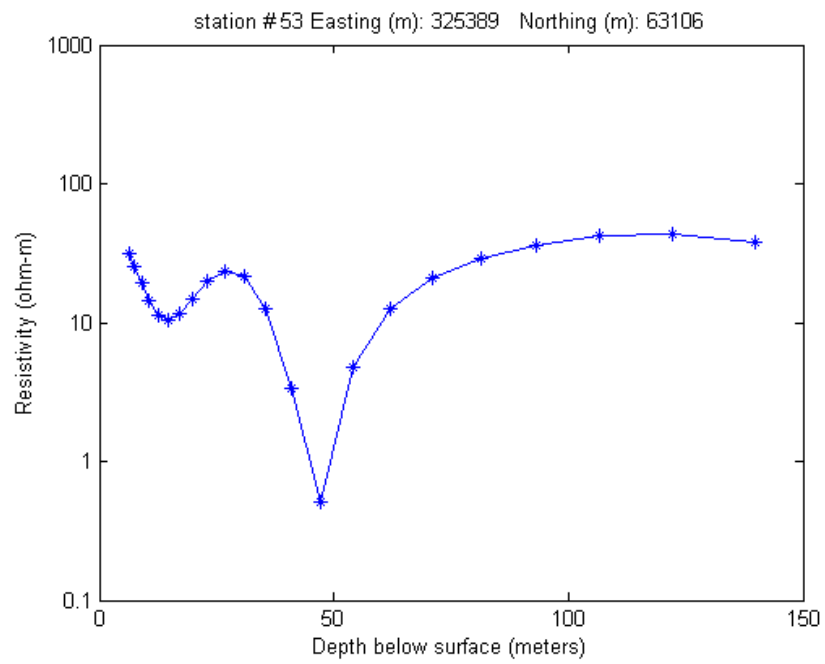
Figure 19: Electrical resistivity model for station 53, note the indication of a possible clay layer at 45 meters depth. Additionally, there is a decrease in resistivity at approximately 20 meters, likely associated with the water table.
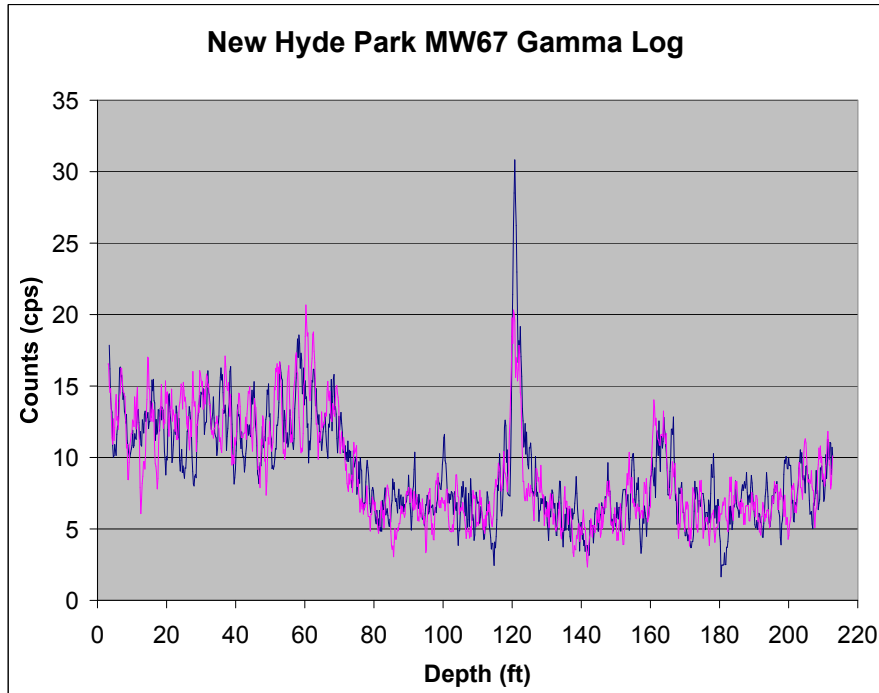
Figure 20: Gamma log for monitoring well MW-67. Note the strong anomaly in the gamma log at a depth of approximately 120 ft (38 m) and a weaker anomaly at a depth of approximately 165 ft (50 m).

4.4   Comparison with Gamma Logs (Where Available)

4.4.1   North 3rd Street

Gamma logs were available for monitoring wells MW-67 (Figure 20) and MW-68 (Figure 21). These wells are located along North 3rd Street (Figure 2), thus corresponding with CSEM line 1. MW-67 and MW-68 are located in the vicinity of CSEM stations 2-3 and 6 respectively.

In well MW-67 there is a strong anomaly in the gamma log at a depth of approximately 120 ft (38 m) and a weaker anomaly at a depth of approximately 165 ft (50 m). Corresponding CSEM stations 2 (Figure 7) and 3 (Figure 8) indicate a strong low resistivity anomaly at a depth of 52 m and 45 m respectively.

In well MW-68 there are no strong anomalies in the gamma log but there

New Hyde Park MW68 Gamma Log
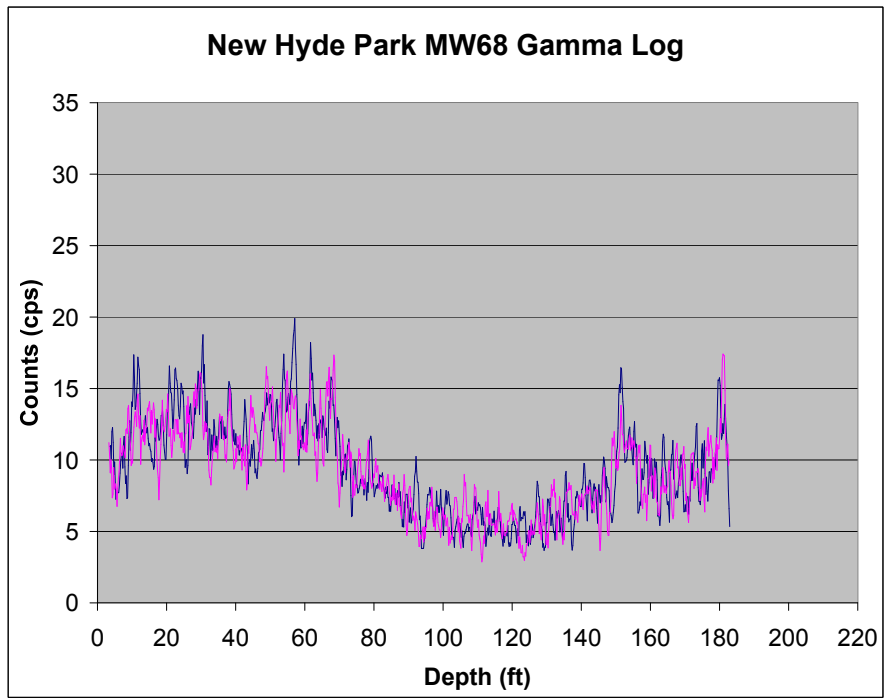
Figure 21: Gamma log for monitoring well MW-68. Note the weak anomaly at a depth of approximately 155 ft (47 m).
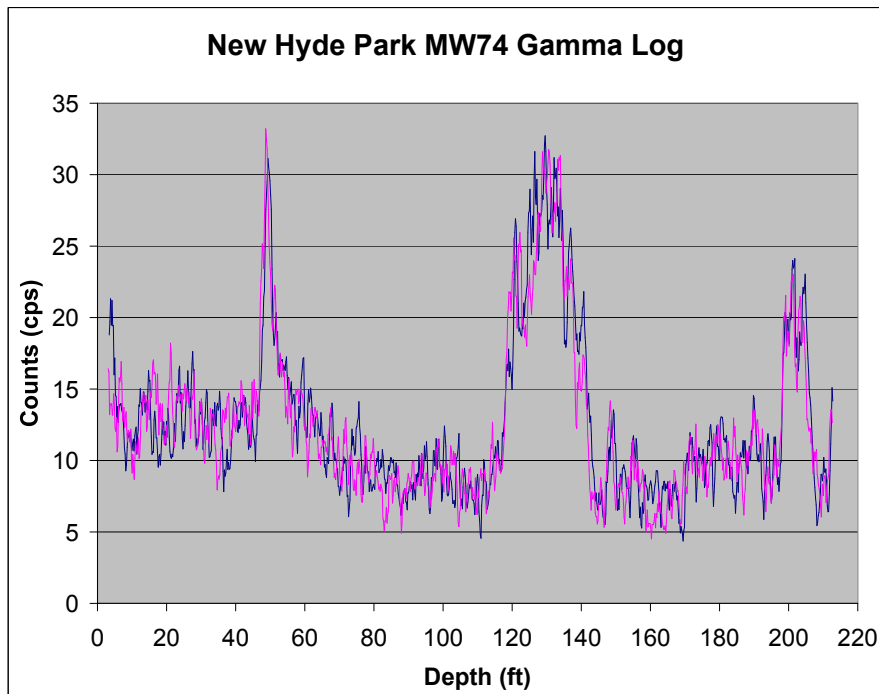
Figure 22: Gamma log for monitoring well MW-74. Note the three strong anomalies at depths of approximately 50 ft (15 m), 130 ft (40 m) and 205 ft (63 m).

is a weak anomaly at a depth of approximately 155 ft (47 m). Corresponding CSEM station 6 (Figure 11) indicates a low resistivity anomaly at a depth of 95 m.

4.4.2 Willis Avenue

Gamma logs were available for monitoring wells MW-74 (Figure 22) and MW-76 (Figure 23). These wells are located along Willis Avenue (Figure 2), thus corresponding with CSEM line 2. MW-74 and MW-76 are located in the vicinity of CSEM stations 31-32 and 37-38 respectively.

In well MW-74 there are three strong anomalies in the gamma log at depths of approximately 50 ft (15 m), 130 ft (40 m) and 205 ft (63 m). Corresponding CSEM stations 31 (Figure 9) and 32 (Figure 16) indicate strong low resistivity anomalies at depths of 45 m and 95 m respectively.
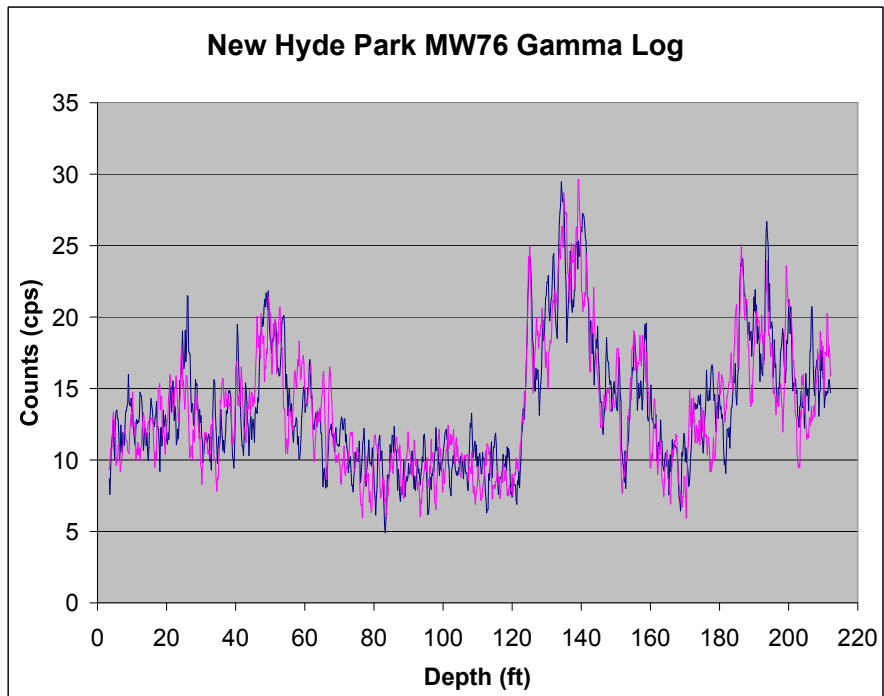
Figure 23: Gamma log for monitoring well MW-76. Note the anomalies at depths of approximately 135 ft (41 m) and 185 ft (56 m).

In well MW-76 there are anomalies in the gamma log at depths of approximately 135 ft (41 m) and 185 ft (56 m). Corresponding CSEM stations 37 (Figure 6) and 38 (Figure 17) indicate low resistivity anomalies at depths of 70 m and 90 m respectively.

5   2D Profiles

In this section, we combine the 1D inversion results from the previous section into 2D resistivity profiles (Figures 24 - 25) along each receiver line. Although many stations along each line are excluded from these profiles due to high data misfit, the 2D profiles do indicate some common features in the geology along each line. Along these 2 profiles, with the exceptions of stations 17 and 32, there is no indication of clay layers shallower than approximately 40 meters. This is in general agreement with the gamma logging results (Figures 20 - 23). Note that the 2D profiles are interpolated in the regions where no 1D models are available. The subsurface structure should be interpreted with caution in these interpolated regions.

6   Discussion and Interpretation

We expected to see at least a small decrease in resistivity at the water table, interestingly this only occurs at stations 16 (Figure 5) and 53 (Figure 19).

The comparisons above indicate that in some cases, the CSEM and the gamma logging have provided similar information. The major difference in the results is that the CSEM indicates only a single conductive anomaly in most cases. There are two explanations for this. First, if there are two clay layers in the subsurface and they are relatively close together, the CSEM results will not be very useful in distinguishing the two layers. Secondly, the noise in the data makes it difficult to resolve thin layers because the data response from a thin layer may not exceed the noise level in the data. In this regard, we would expect that the CSEM models are indicating the strongest anomalies in this depth range, while weaker anomalies are overcome by noise. These strongest anomalies are likely due to thicker, more laterally extensive clay layers, which may have the strongest influence on groundwater flow.

The source strength of 1.4 to 3.8 Amperes injected current could be increased somewhat by deploying a more powerful generator and constructing
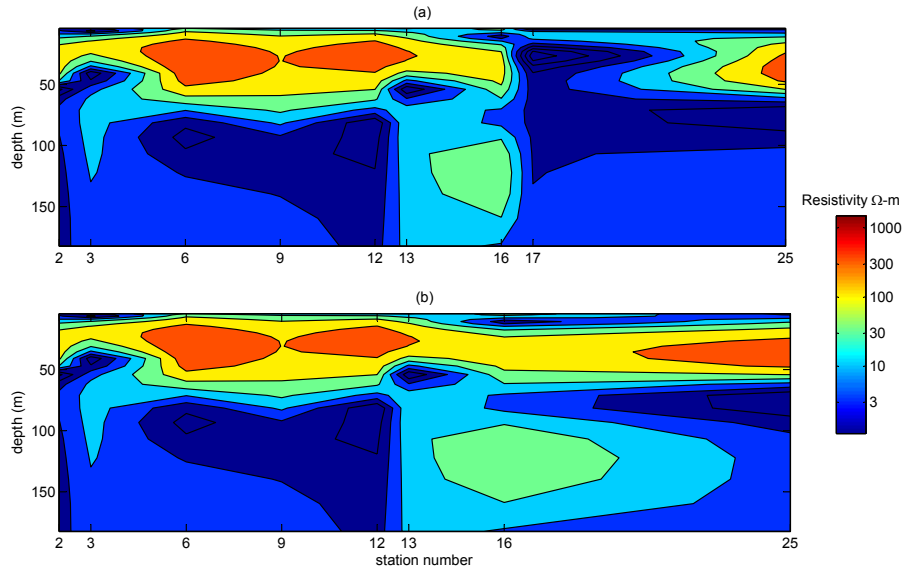
Figure 24: Plot (a): 2D electrical resistivity profile from stitched 1D inversion along Line 1. Only those stations described in the previous section are included in this profile, i.e. stations with poor data fit are excluded. Clay layer depths appear highly variable at this site, thus the profiles do not depict a monotonous layered structure, but rather a complex structure with discontinuous conductive layering at various depths. Plot (b): Same as plot (a) except with station 17 removed. This plot exhibits more lateral continuity. Based on this apparent improvement (i.e., less blocky structure) in the image, the shallow clay layer evident in station 17 is likely an inversion artifact and not resulting from actual subsurface structure.
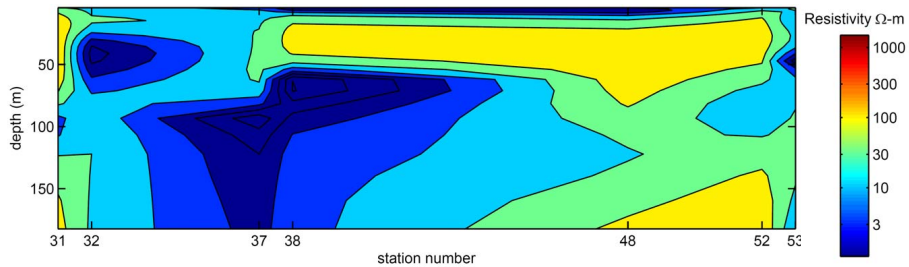
Figure 25: 2D electrical resistivity profile from stitched 1D inversion along Line 2. As in Figure 24, stations with poor data fit are excluded.

deeper/larger electrode pits. However, it should be noted that this source transmission was more than adequate based on the survey geometry and the depth of interest. In other words, injecting more current would probably slightly improve the signal to noise ratio but the signal would remain strongly affected by the near surface sources of electrical noise.

7   Recommendations

Cultural noise sources at the New Hyde Park site complicate the data analysis process. When/if future data acquisition is planned, there should be a focus on minimizing or at least quantifying the sources of electrical noise at the site. Existing monitoring wells may be useful as EM receiver locations. By placing the receivers downhole, much of the noise introduced by the very near surface utilities might be eliminated. This would also allow for a direct comparison and/or constraint of the geophysical results to borehole lithology logs or other borehole survey information such as the natural gamma logging. Comparing the downhole EM data with data collected at the surface in the same location would be very useful in quantifying the effect of near surface noise sources. We also recommend completing natural gamma logging in all accessible existing and new wells and, where possible, collect lithologic samples to compare with the gamma logs for variations in grain size and/or mineralogy that can explain the variations in count rates.

8   Acknowledgments

Appendix A: Controlled Source Electromagnetics (CSEM)

Controlled Source Audio-Frequency Magnetotellurics is a frequency domain electromagnetic (EM) sounding technique. A CSEM survey typically uses a grounded horizontal electric dipole approximately one to two kilometers in length as a source. Measurements of electric and magnetic field components are made at stations located at least four skin depths away from the transmitter to approximate plane wave characteristics of the source. Data are acquired in a broadband frequency range that is sampled logarithmically from 0.1 Hz to 10 kHz. The usefulness of CSEM soundings is to detect and map electrical conductivity contrasts in the top two to three kilometers of the Earth's surface. Some practical applications that CSEM soundings have been used for include mapping ground water resources (Zonge *et al.*, 1985); mineral/precious metals exploration (Routh & Oldenburg, 1999; Phillips *et al.*, 2001); geothermal reservoir mapping (Bartel & Jacobsen, 1987; Sandberg & Hohmann, 1982; Miller *et al.*, 2006); petroleum exploration (Nekut & Spies, 1989; Hughes & Carlson, 1987); and geotechnical investigations (He *et al.*, 2006; Unsworth *et al.*, 2000). Higher frequency data can be used to image shallow features and lower frequency data are sensitive to deeper structures (Zonge & Hughes, 1991). The behavior of the electric and magnetic fields is described by the coupled Maxwell's equations:

$$\nabla \times E - i\omega\mu H = 0, \tag{1}$$

$$\nabla \times H = \sigma E + J_s, \tag{2}$$

where E is the electric field intensity (V/m); H is the magnetic field intensity (A/m); μ is the magnetic permeability $(Wb/A - m)$; σ is the electrical conductivity (S/m); ω is the angular frequency $(1/s)$ and J_s is the source current (A/m^2). The observed electric field has a primary component from the galvanic current and an inductive component arising from the time varying magnetic field generated by the source. The decoupled equation for the electric field can be written as:

$$E = -\nabla\phi - i\omega A, \tag{3}$$

where ϕ is a scalar potential and A is a vector potential. From this equation it can be seen that at low frequencies the electric field is dominated by the galvanic character of the source and at higher frequencies the contribution of the inductive character of the source takes on greater importance.

Appendix B: 1D CSEM Inversion

We use an unconstrained Gauss-Newton method with positivity to invert the data in 1D (Routh & Oldenburg, 1999). The inverse problem can be stated as:

$$Minimize: \quad \phi_m = \alpha_s \|W_s(m - m_0)\|^2 + \alpha_z \|W_z(m - m_0)\|^2, \qquad (4)$$

$$Subject\ to: \quad \phi_d = \|W_d(d^{obs} - \mathcal{F}(m))\|^2 = \phi_d^{target}, \qquad (5)$$

where $m \in R^{M \times 1}$ is the model vector; $m_0 \in R^{M \times 1}$ is the reference model vector; W_s and $W_z \in R^{M \times M}$ are the smallest and flattest model weighting matrices respectively; α_s and α_z are parameters controlling the relative contribution of the smallness and flatness components; $d^{obs} \in R^{N \times 1}$ is the data vector; $\mathcal{F}(\cdot)$ is the nonlinear forward modeling operator; W_d is the data weighting matrix and ϕ_d^{target} is the desired level of data misfit determined by the χ^2 misfit criterion. The 1D inversion does not account for differences in elevation between the transmitter and the receiver but instead assumes that both are at the same elevation. Also, use of the 1D inversion is most appropriate when the conductivity structure is horizontally layered, with smooth and minor lateral variations. Violation of these two assumptions will result in some artifacts in the inverted models and motivates further analysis using 2D or 3D inversion.

Appendix C: Natural Gamma Logging

Natural gamma logs were run in 10 monitoring wells in the New Hyde Park area during August 21-23, 2006 with a Mount Sopris narrow diameter tool (HLP-2351). The objective of the logging was to identify silt- or clay-rich zones in a given well and compare these occurrences among wells to see if fine-grained layers or lenses can be traced in the shallow sand aquifer in the New Hyde Park area.

Logged wells were: ML82D, ML84S, MW21, MW27, MW63, MW67, MW68, MW72, MW74, and MW76. The logging tool was run in the central riser of these wells at about 15 ft/min with data collected at 0.1 ft intervals. Depth to water in all wells was between 61 and 67 ft at the time of logging (August 21-23, 2006). Records were collected from downward and upward logging runs and they correlate very well (e.g., Figures 20-23 and 26-31 show

logs with 10-point moving averages of the data). Data for all runs are given in the CD accompanying this report.

Overall, the distribution of wells logged for this investigation form a transect approximately parallel to Hillside Avenue with one or two wells at one- to two-block intervals between North 5th Street to the ENE and Willis Avenue to the WSW. Well depths range from about 120 ft to about 220 ft with all but one well deeper than 150 ft from land surface. Low topographic relief in the area permits discussion of subsurface correlation using well depths.

It is known from auger cuttings records that unconsolidated sand dominates the investigated depths of wells in this area. Results from the logging indicate that the upper 220 ft of the subsurface can generally be divided in to an upper sand unit from near land surface to about 75 ft with counts ranging between 10-15 cps (counts per second), and a lower sand unit from bout 75 ft to at least 180 ft with counts ranging between 5-10 cps. At this point it is not known if the difference in count rate between these two sand units is due to relative abundances of silt or clay or to mineralogical differences.

Local increased count rates in the logs are tentatively interpreted as intervals with increased fines content. In the upper sand unit, only two wells (MW74 and MW76) have intervals of increased count rates; these wells are near each other on Willis Avenue at the WSW end of the transect. The interval with increased counts occurs from about 45-55 ft depth. In the lower sand unit, intervals with elevated count rates occur in several wells at depths of about 120 ft, 170 ft, and 200 ft.

At about 120 ft (in the lower sand unit), wells ML84S, MW21, and MW67 show a thin zone, wells MW27 and MW63 have two thin zones in close vertical proximity, and wells MW74 and MW76 have 20 ft thick zones. The close lateral proximity of wells with similar variations of occurrence (i.e., one thin zone, two thin zones, or one thick zone) strongly suggest that these occurrences are not random anomalies but rather are local expressions of the same phenomenon (i.e., cause for elevated gamma counts) and may be discontinuous lenses of relatively fine-grained sediments.

At about 170 ft (in the lower sand unit), only MW63 and MW72 have 20 ft-thick intervals of elevated count rates and these wells are separated laterally by about 800 ft. There is an increase in count rate near the bottom of well MW21 which is near well MW63, but well MW21 does not reach 170 ft depth and it is speculative as to whether this occurrence in MW21 is related to or continuous with that at MW63.

Only four wells reach a depth of >200 ft (i.e., in the lower sand unit) but
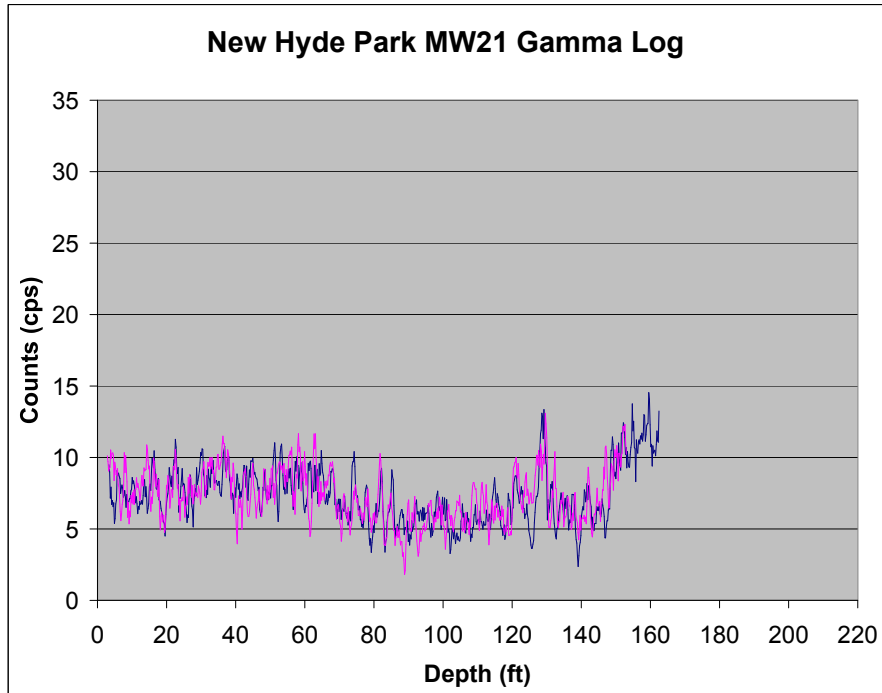
Figure 26: Gamma log for monitoring well MW-21.

three of these (MW72, MW74, MW76) are adjacent and near the WSW end of the transect, and they each have a 10-20 ft-thick interval with elevated gamma count rate at about 190 ft or 200 ft depth.

Considering the gamma log results together, it is reasonable to hypothesize that there are relatively fine-grained lenses and/or layers of varying continuity (i.e., one local occurrence at about 50 ft depth with known extent <400 ft diameter but which could continue to the W, to perhaps the full length of the studied area for the interval at about 120 ft which however is not of uniform thickness and which is also locally absent in the study area). With the stated hypothesis, the elevated count rate occurrences present targets for relatively high electrical conductivity anomalies in results from electrical geophysical methods.
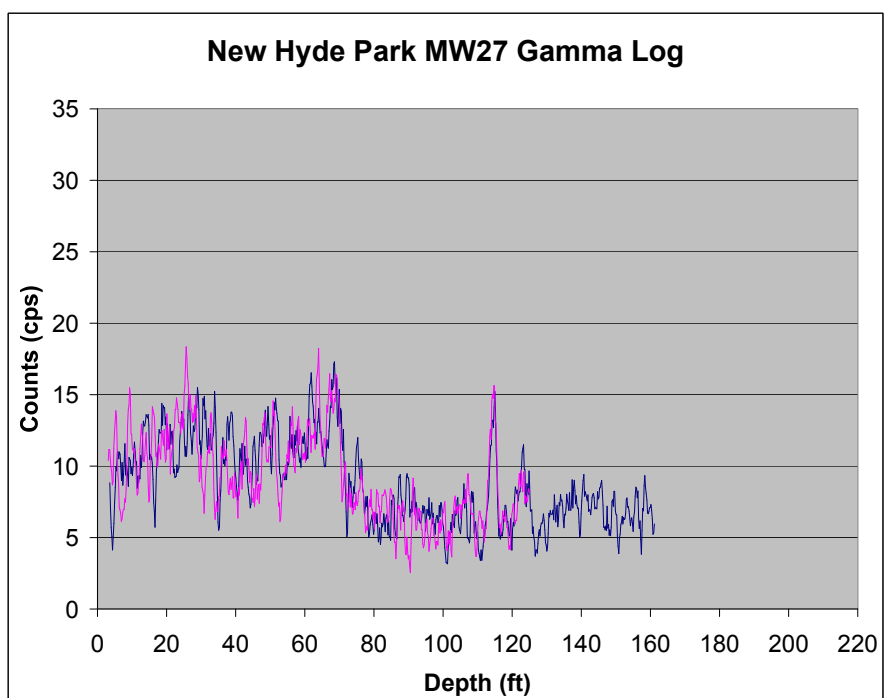
Figure 27: Gamma log for monitoring well MW-27.
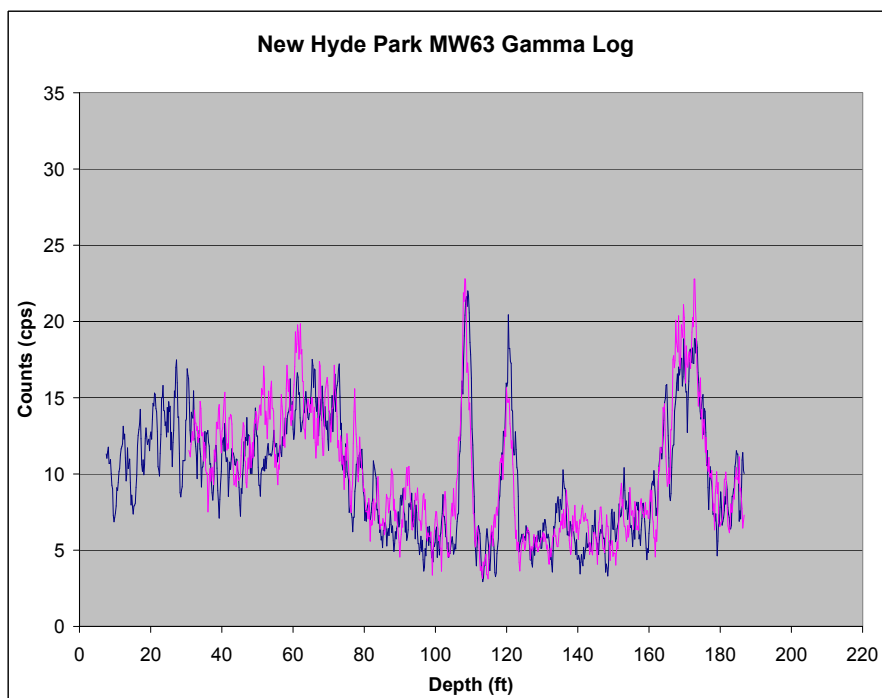
Figure 28: Gamma log for monitoring well MW-63.
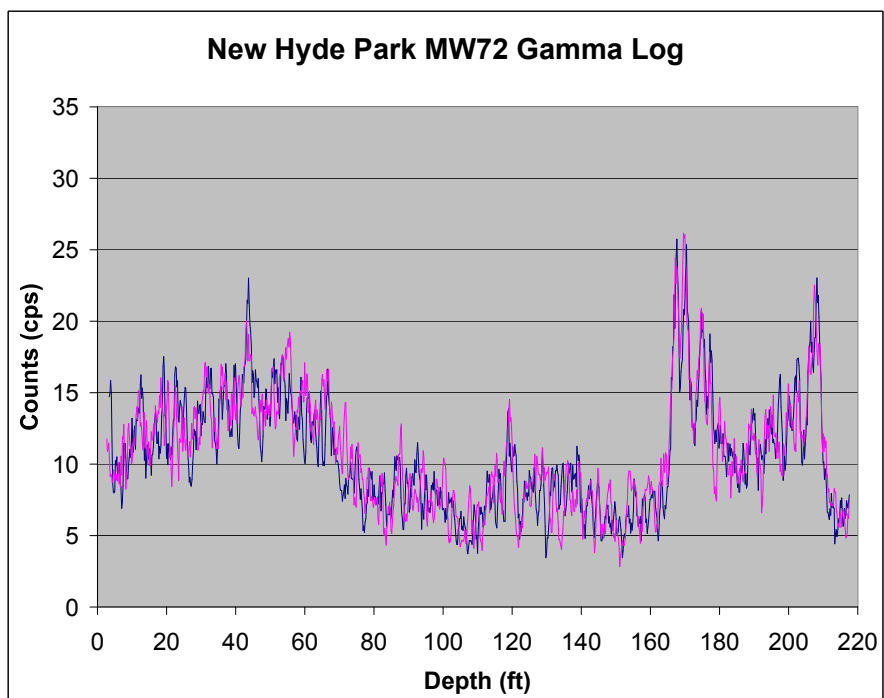
Figure 29: Gamma log for monitoring well MW-72.
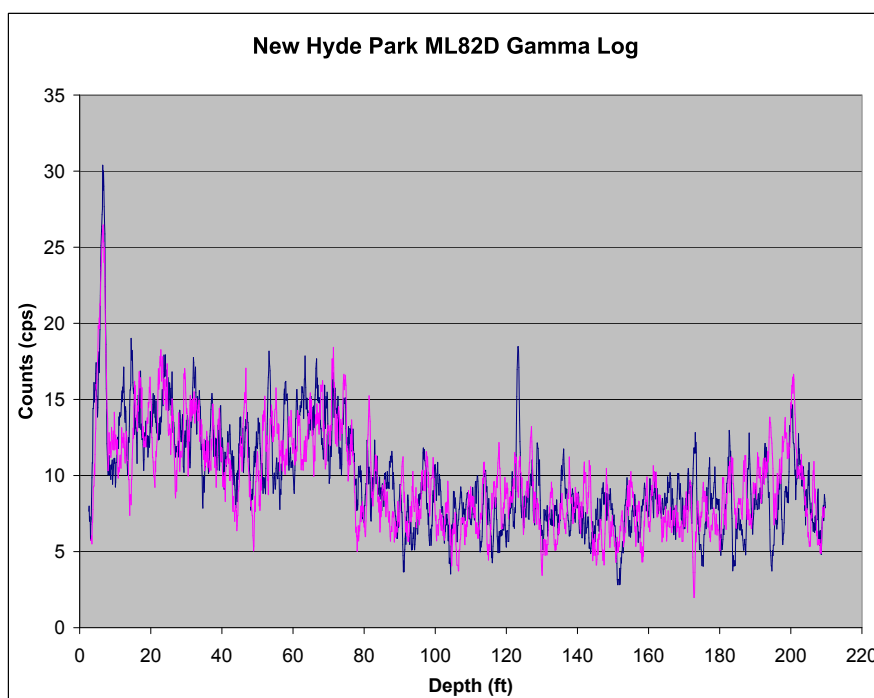
Figure 30: Gamma log for monitoring well ML-82D.
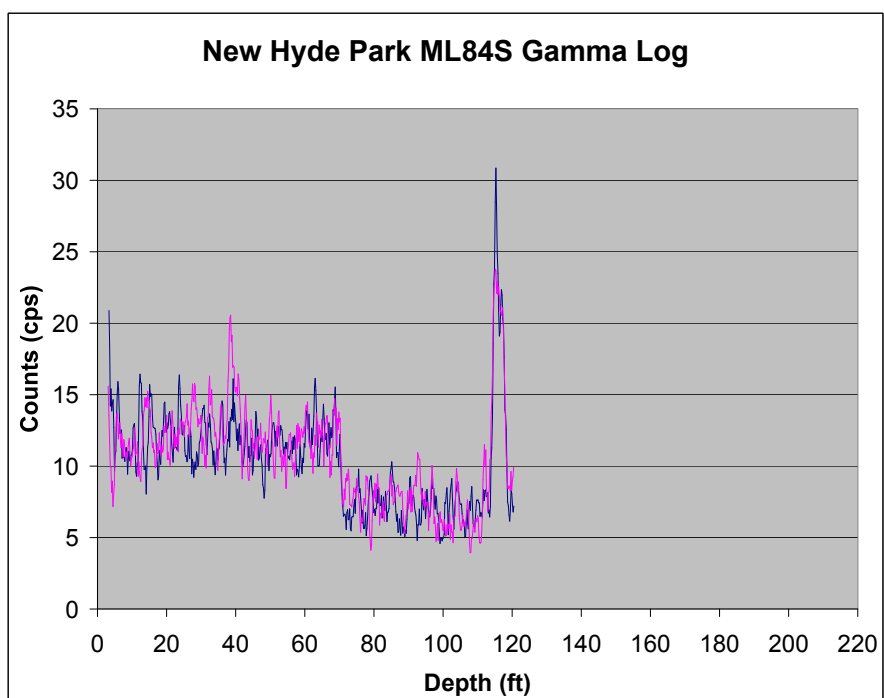
Figure 31: Gamma log for monitoring well ML-84S.

References

Bartel, L. C., & Jacobsen, R. D. 1987. Results of a controlled-source audiofrequency magnetotelluric survey at the Puhimau thermal area, Kilauea Volcano, Hawaii. *Geophysics*, **52**, 665–677.

He, Lanfang, Feng, Minghai, He, Zhanxiang, & Wang, Xuben. 2006. Application of EM Methods for the Investigation of Qiyueshan Tunnel, China. *Journal of Environmental and Engineering Geophysics*, **11**(2), 151–156.

Hughes, L. J., & Carlson, N. R. 1987. Structure mapping at Trap Spring Oilfield, Nevada, using controlled-source magnetotellurics. *First Break*, **5**(11), 403–418.

Miller, C., Routh, P., Donaldson, P., & Oldenburg, D. 2006. Imaging a geothermal system using controlled-source electromagnetics. *Geothermal Resources Council Transactions Bulletin*, **30**, 447–451.

Nekut, A. G., & Spies, Brian R. 1989. Petroleum Exploration Using Controlled-Source Electromagnetic Methods. *Proceeding of the IEEE*, **77**(2), 338–362.

Phillips, N., Oldenburg, D. W., Chen, J., Li, Y., & Routh, P. S. 2001. Cost-effectiveness of geophysical inversions in mineral exploration: applications at San Nicolas. *Leading Edge*, **20**(12), 1351–1360.

Routh, P., & Oldenburg, D. 1999. Inversion of controlled source audio-frequency magnetotelluric data for a horizontally layered Earth. *Geophysics*, **64**, 1689–1697.

Sandberg, S. K., & Hohmann, G. W. 1982. Controlled-source audiomagnetotellurics in geothermal exploration. *Geophysics*, **47**, 100–116.

Unsworth, Martyn J., Lu, Xinyou, & Watts, M. Don. 2000. CSAMT exploration at Sellafield: Characterization of a potential radioactive waste disposal site. *Geophysics*, **65**(4), 1070–1079.

Zonge, K. L., & Hughes, L. J. 1991. Controlled source audio-frequency magnetotellurics. *in Nabighian, M. N., Ed., Electromagnetic methods in applied geophysics*, 713–809.

Zonge, K. L., Figgins, S. J., & Hughes, L. J. 1985. Use of electrical geophysics to detect sources of groundwater contamination. *Pages 147–149 of: SEG Expanded Abstracts.* SEG.